ON THE SUFFICIENCY OF CLASSICAL RESPONSE MODELS IN PREDICTING THE DYNAMIC BEHAVIOR OF FLEXIBLE STRUCTURES

Demian G. da Silva
PhD Student
demian@sc.usp.br

Paulo S. Varoto
Associate Professor
varoto@sc.usp.br

University of São Paulo, Campus of São Carlos
Department of Mechanical Engineering
Laboratory of Dynamics and Mechatronics
Av. Trabalhador São-Carlense 400, CEP: 13566-590, São Carlos, Brazil

Abstract

The sufficiency of classical response models in predicting the dynamic behavior of flexible structures has been investigated theoretically and experimentally. Important issues involving nonlinear dynamic behavior exhibited by the test structure are addressed in a complete sense for a structure modelled as a single degree of freedom system. The major goal is to perform an analytical and experimental analysis of the parametric resonance phenomenon as well as to discuss limitations of currently employed modal testing methods when this phenomenon occurs in physical systems. A very simple structure has been chosen as the structure under test which consists of a very flexible cantilever beam carrying a tip mass. Analytical models have been developed for the system considering both the classical and the well known modal analysis approach for the case of infinitesimal amplitudes and perturbation technique when finite amplitudes are concerned. Analytical solutions are obtained for both models in order to show limitations of the classical approach. A detailed experimental study is carried out on the test structure where several tests are conducted using standard modal testing techniques as well as nonconventional testing procedures in order to validate most of the results obtained theoretically.

Nomenclature

m_o	Lumped mass
L	Beam length
$u_o(t)$	Lateral displacement of the lumped mass
$u(z,t)$	Lateral displacement of the beam elastic axis
$w_o(t)$	Axial contraction of the lumped mass center
$W(t)$	Excitational displacement at the base
X, Y, Z	Newtonian cartesian reference frame
T	Kinetic energy
U	Strain energy
E	Elastic (Young's) modulus
I_y	Cross-sectional moment of inertial about y axis
$q(t)$	Generalized co-ordinate
ρ	Curvature radius
ds	Infinitesimal distance on the beam
dz	Infinitesimal distance at z direction
$d\theta$	Infinitesimal angle
κ	Curvature of the beam
g	Acceleration of gravity
Q_{nc}	Generalized force
c_1, c_2	Damping coefficients
O'	Center of the curvature
k	Linear stiffness of the system
ζ	Damping ratio
ω_n	Linear undamped natural frequency
ω_d	Linear damped frequency
T_n	Linear undamped natural period
A, B	Geometrical constants
$f(z)$	Linear mode shape function
F_x	External force excitation
$H(i\Omega_e)$	Receptance FRF
$A(i\Omega_e)$	Accelerance FRF
$OTR(\epsilon^1 QB, \phi)$	Orthogonal Transmissibility Ratio

1 INTRODUCTION

Success in engineering new products depends on a variety of important issues such as introducing innovations as for example in terms of geometry and new materials that will ultimately lead to better, cheaper, and faster machines and structures. Recently, newspapers advertised that a major aircraft manufacturer has a new prototype on the drawing board that, once in production in a few years from now, will become the largest commercial aircraft available, being able to fly more than five hundred people in a single non stop flight. Almost at the same time it was advertised that another giant in the commercial aircraft manufacturing business plans to stretch one of its best seller models in order to accommodate more than six hundred passengers ! Similarly, major automobile companies around the globe have been recently putting a lot of effort on new design strategies aiming to achieve higher levels of comfort and reliability in modern automobiles. Generally speaking, modern machines have become lighter and frequently more flexible, being susceptible to higher deflection and acceleration levels when exposed to different dynamic environments. Thus, design and test personnel must be aware that not only a detailed knowledge of the dynamic behavior of the structure under study is required but also the reduction in weight and increased flexibility can impose limitations on the use of currently employed linear modal analysis techniques. Particularly, the presence of nonlinear effects in the system's dynamic behavior have proven to be of major interest in the modal and vibration testing areas primarily due to the peculiar circumstances that these effects might occur in practical applications, notoriously in testing situations. Therefore, the major goal of this paper is to address important issues involving nonlinear vibratory behavior as well as situations where the classical modal analysis approach is insufficient to fully describe the physical phenomena involved in innovative engineering solutions.

The classical modal analysis approach has been an important engineering tool to predict the dynamic behavior of structures. Since 1940's when the foundations of modal analysis were first established, many improvements have been achieved in both analytical and experimental routes so that today a broad range of techniques are available in order to identify modal models and evaluate their performance in predicting response levels to different inputs, model validation, updating of analytical dynamical models, development of experimentally based dynamical models, and structural modification. In addition to the improvements obtained in the analytical tools, good progress has also been reached in the areas of instrumentation and commercially available computer programs for modal identification and model updating. The mathematical foundations of the classical modal analysis principles are based on three basic assumptions: (i) the structure is linear and the principle of superposition holds, which means that the system's dynamic response is given in terms os a set of linearly independent mode shapes; (ii) the structure obeys Maxwell's reciprocity theorem; (iii) the structure is time-invariant. Provided these assumptions are met it is possible to use the standard modal testing principles in order to build a reliable mathematical model of the test structure.

However, in the presence of nonlinear effects the assumptions listed above do not hold and the structure does not present a

unique dynamic response for different levels of the input or initial conditions. In this case the application of concepts from the linear theory will very often conduct to misleading results. The general theory of nonlinear vibrations usually classifies nonlinearities according to several sources [13]: material, when the stresses are nonlinear function of the strains; geometric, stems from nonlinear strain-displacement relationships; friction, when the dissipative forces are nonlinear functions of the displacements and/or velocities; and inertial. Although these sources of nonlinear effects are found in many practical applications, there is one type of nonlinear effect that despite being very important in the general structural vibration context, usually is not a source of much attention in modal testing and it is called parametric resonance. Faraday [3] in 1883 was probably one of the first to observe this phenomenon by noticing that the wine in glass presented a strong oscillation at a frequency approximately half of the exciting frequency provided by the movement of the finger around the edge of the glass. Only in 1887, Lord Rayleigh [3] provided a mathematical explanation the phenomenon previously observed by Faraday which was named parametric resonance ([2], [3],[14]).

Beliav, 1924, apparently was the first in providing an analysis of the parametric resonance for a purely structural system that consisted a straight elastic column pinned at both ends and subjected to an axial periodic sinusoidal force at a constant excitation frequency. The results shown that the column could vibrate with half of the original excitation frequency if this frequency was close to a bending natural frequency of the column, even if the amplitude of the applied force was kept below of the column buckling load [3].After Believ, some other authors have analyzed the parametric resonance in other kinds of structural elements. Einaudi in 1936 was the first to study this phenomenon in plates and Bublik and Merkulov in 1942 were the pioneers investigating the problem in cylindrical shells [3].Eventhough the parametric resonance phenomenon have been a source of interest and investigation for several decades, many researchers and engineering practitioners are still not completely aware about the consequences of this dangerous phenomenon.

As previously pointed out in the beginning of this section, the major goal of this paper is to perform a analytical and experimental analysis of the parametric resonance phenomenon as well as discuss limitations of currently employed modal testing methods when this phenomenon occurs in physical systems. A very simple structure was chosen as the structure under test which consists of a very flexible cantilever beam carrying a tip mass. Analytical models are built for the system considering both the classical and well known modal analysis approach for the case of infinitesimal amplitudes and perturbation techniques when finite amplitudes are concerned. Analytical solutions are obtained for both models in order to show limitations of the classical approach. Experimental tests are conducted on the prototype in order to validate most of the results obtained theoretically.

2 THE STRUCTURE UNDER INVESTIGATION

In order to discuss the parametric resonance phenomenon from the experimental and analytical viewpoints, the structure shown in fig.1 was built. It is composed of a slender stainless steel ASTM A240, with dimensions of $100\,\mathrm{mm}$ in length, $20\,\mathrm{mm}$ in width and $1\,\mathrm{mm}$ in thickness. The lumped-mass is composed of carbon steel ASTM A36, with dimensions of $10\,\mathrm{mm}$ in length, $40\,\mathrm{mm}$ in width and $20\,\mathrm{mm}$ in height. On opposite end the beam is clamped to a rigid steel base that was built from carbon ASTM A36 steel.

Some basic assumptions are made in order to simplify the analysis. First, the thickness of the beam is small compared to the length so that the effects of shearing strain and rotatory inertia of the beam can be neglected. Also it is assumed that the material of the beam obeys the constitutive Hook's law, is isotropic and there is neither plastic strain or internal heat generate during the vibration. At the end, the beam is considered as massless. According to these assumptions, the first level of analysis is performed in which the dynamics of the structure under investigation is analyzed through classical infinitesimal amplitudes.

3 FIRST LEVEL OF ANALYSIS: INFINITESIMAL AMPLITUDE OF VIBRATION

The classical modal analysis theory consists of three stages that must be accomplished in order to assess the structure's dynamic response [4]. The first stage consists of obtaining a spatial description of the structure in terms of mass, stiffness and eventually damping matrices. This stage is usually performed by some discretization procedure, and in this case de Finite Element Analysis (FEA) technique is widely employed. Once the spatial characteristics are determined, they are used in the second stage that consists in determining the structure's modal model, composed by the natural frequencies, normal mode shapes and modal damping ratios. These properties are very important since they allow the calculation of the structure's Frequency Response Functions (FRFs). Finally, the FRFs are used in the third and last stage that consists

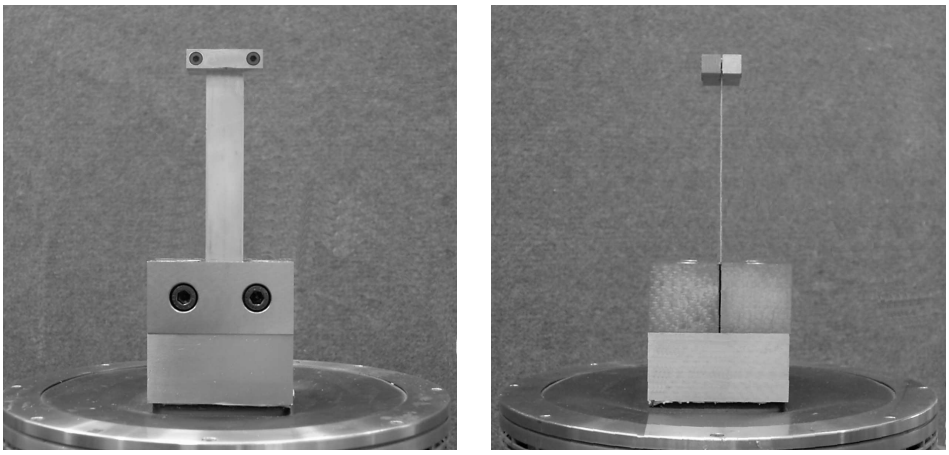

(a) **(b)**

Figure 1 - Physical system under investigation: (a) frontal view; (b) lateral view.

in determining the structure's response model to a given prescribed inputs. In this case, the analysis is usually carried out in the frequency domain where the output is obtained by multiplying the Fourier transform of input by the system's FRF matrix. The next section presents a brief review of this classic approach.

3.1 Spatial Model for Transverse Motion

Several approaches are commonly used to derive the classical spatial model, such as, the Newtonian mechanics, d'Alembert's principle, and the Lagrangian mechanics [9]. In the present work, the Lagrangian mechanics has been chosen for deriving the equation of motion for forced vibrations of the test structure shown in fig.2. In addition to the assumptions made before, it is also considered that the beam's transverse vibration is purely planar and completely described in the OZX plane since the lumped mass is symmetric with respect to the centerline and the beam is kept short (less than thirty times the beam's width) then the torsional modes can be neglect in the analysis. These assumptions proved to be consistent with observations made in the laboratory during the tests. Furthermore, the assumption of infinitesimal transversal amplitudes of vibration is also considered in this analysis.

Based on the assumptions made in the previous sections, the system's kinetic energy comes uniquely from the lateral velocity $\dot{u}_o(t)$ of the lumped mass. Also by considering the structure as a scleronomic system [17] the kinetic energy function is given by

$$T = \frac{1}{2} m_o \dot{u_o}^2 \tag{1}$$

whereby the dot denotes the first time derivative of the variable considered.

Based on the assumption of infinitesimal amplitude of vibration, the strain energy or potential energy U of the system is given by ([2],[5],[15]),

$$U = \frac{1}{2} E I_y \left[\int_0^L \left(u^{"} \right)^2 dz \right] \tag{2}$$

whereby the primes denotes the partial derivative with respect to z, E is the elastic (Young's) modulus and I_y is the cross-sectional moment of inertial about the y axis.

The general lateral displacement $u(z,t)$ can be related to the lateral displacement of the lumped-mass center $u_o(t)$ by a Galerkin representation based on the linear shape function $f(z)$ defined as

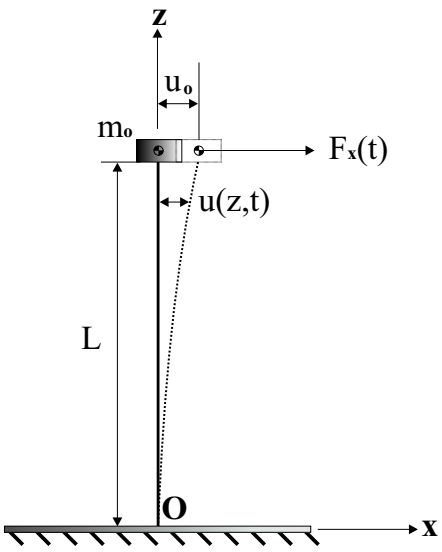

Figure 2 - Physical model of the structure under investigation under infinitesimal displacement u_o hypothesis.

$$u\left(z,t\right)=f\left(z\right)u_{o}\left(t\right) \tag{3}$$

Substitution of eq.3 into eq.2 leads to the following result

$$U=\frac{1}{2}EI_{y}\left[\int_{0}^{L}\left(f^{"}\right)^{2}dz\right]u_{o}^{2} \tag{4}$$

which describes the strain energy in terms of the displacement at the lumped-mass center $u_o(t)$. For this case, there is not motion in the z direction and consequently the gravitational potential energy contribution for the total potential energy of the system is null.

In this level of analysis, it will be considerer the action of two nonconservative forces, or forces that are not obtained from the potential function U. The first nonconservative force, represents the structural damping and is modelled in terms of generalized coordinates such as $c_1\dot{u_o}$, in which c_1 represents the linear viscous damping coefficient. The second nonconservative force represents a standard forced excitation term chosen as a unit-amplitude, mono-component, sinusoidal force $F_x\left(t\right)$ applied at the center of gravity of the lumped mass and oriented along the x direction. The external excitation $F_x\left(t\right)$ acts in the positive direction of the virtual transversal displacement δu_o, whereas the linear viscous damping force is oriented in the negative direction.

Therefore, the nonconservative virtual work δW_{nc}, in which is done on the system is given by $\delta W_{nc}=\left[F_x(t)-c_1\dot{u_o}\right]\delta u_o$. Since the nonconservative virtual work is defined as a function of the nonconservative generalized force Q_{nc} as $\delta W_{nc}=Q_{nc}\delta u_o$, therefore the nonconservative generalized force Q_{nc} is obtained as

$$Q_{nc}=\frac{\delta W_{nc}}{\delta u_o}=F_x(t)-c_1\dot{u}_o \tag{5}$$

For this system, the Lagrange's equation of the motion thus become

$$\frac{d}{dt}\left(\frac{\partial T}{\partial\dot{u}_o}\right)-\frac{\partial T}{\partial u_o}+\frac{\partial V}{\partial u_o}=Q_{nc} \tag{6}$$

By performing each term of the Lagrange's equation, substituting the result in the eq.6 and assuming that the external excitation can be written as $F_x\left(t\right)=F_oe^{i\Omega_e t}$ the spatial model for transverse motion of the system proposed under those specifics conditions is derived, such final result is given as

$$m_o\ddot{u}_o + c_1\dot{u}_o + \underbrace{\left\{EI_y\left[\int_0^L \left(f''\right)^2 dz\right]\right\}}_{k} u_o = F_o e^{i\Omega_e t} \tag{7}$$

whereby k is the linear transversal stiffness of the structure.

In order to further correlate this theoretical model with experimental results, it is interesting to describe eq.7 as function of the modal damping ratio ζ. By definition [16], the linear viscous damping coefficient c_1 can be written as a function of the damping ratio ζ, the lumped mass m_o and, the undamped natural frequency ω_n as $c_1 = 2\zeta m_o \omega_n$. Substituting c_1 and dividing by m_o, eq.7 can be written as

$$\ddot{u}_o + 2\zeta\omega_n\dot{u}_o + \omega_n^2 u_o = \frac{F_o}{m_o} e^{i\Omega_e t} \tag{8}$$

whereby the undamped natural frequency ω_n is given by

$$\omega_n = \sqrt{\frac{EI_y\left[\int_0^L \left(f''\right)^2 dz\right]}{m_o}} \tag{9}$$

In this item, the transversal forced spatial model of the proposed system has been derived by applying the Lagrange's equation under the condition of infinitesimal amplitude and under the action of a external excitation. From this spatial model, in the next item the transversal forced response model will be derived.

3.1.1 Transversal Forced Response Model of the Structure

In order to determine the system's steady state harmonic response it is simply assumed that the solution of eq.8 is ([4], [6])

$$u_o = U_o e^{i\Omega_e t} \tag{10}$$

Substitution of eq.10 into eq.8 gives

$$\left[\left(i\Omega_e\right)^2 + 2\zeta\omega_n\left(i\Omega_e\right) + \omega_n^2\right] U_o e^{i\Omega_e t} = \frac{F_o}{m_o} e^{i\Omega_e t}$$

Cancellation of the $e^{i\Omega_e t}$ and solution for the response U_o results in

$$U_o = \frac{1}{m_o\left[\left(i\Omega_e\right)^2 + 2\zeta\omega_n\left(i\Omega_e\right) + \omega_n^2\right]} F_o = H\left(i\Omega_e\right) F_o \tag{11}$$

The $H\left(i\Omega_e\right)$ is the reeptance FRF, relating the transversal displacement response of the structure per unit of excitation force applied at the beam's tip mass for each excitation frequency $i\Omega_e$. It is very common in the experimental route of vibration measurements to express the input/output relationships either in terms of velocity or acceleration instead of displacement. Specifically, for the case of acceleration, the forced response model, called of accelerance $A\left(i\Omega_e\right)$ relates the acceleration of the system per unit of excitation force at each frequency $i\Omega_e$. By definition ([4], [7]) the relationship between the receptance and accelerance is given by

$$A\left(i\Omega_e\right) = \left(i\Omega_e\right)^2 H\left(i\Omega_e\right) = \frac{\left(i\Omega_e\right)^2}{m_o\left[\left(i\Omega_e\right)^2 + 2\zeta\omega_n\left(i\Omega_e\right) + \omega_n^2\right]} \tag{12}$$

The result shown in eq.12 will be further recalled in the experimental analysis of the test structure.

3.2 Experimental Forced Response For Transverse Vibration

This section describes the experimental analysis performed on the test item previously defined in fig.1. The main goal here is to determine basic properties of the test item such as the first bending natural frequency and modal damping ratio. In order to accomplish this task, standard modal testing procedures are employed. The test item is excited in a broad range of frequencies through some excitation mechanism and the output acceleration response is measured through piezoelectric miniature accelerometers. The applied input force is also measured by a force transducer. Input and output signals are then processed using standard digital signal processing techniques in order to get the system's FRF. From the measured FRF it is possible to obtain modal parameters using a modal identification procedure.

Several excitation methods were employed in measuring the FRF of the system shown in fig.1. Initially a test was conducted using a electrodynamic shaker attached to the beam's tip mass of the system shown in fig.1. This test procedure was considered insatisfactory since the structure is very flexible and significant exciter-structure interaction was observed specially in the vicinity of the structure's natural frequencies. The force drop off has altered the measured FRF consequently the identified modal parameters. Then a second test was performed by using an impact hammer. Although very versatile, the impact test also presented problem, mostly due to unmeasured double impacts, again, due to the high flexibility of the beam. The results from this test were considered poor as well.

In order to solve the problem of providing a reasonable excitation signal to the test item, the step relaxation technique ([7]) was employed. The step-relaxation method requires that initially a static load be applied to the structure and then suddenly released. This excitation mechanism is usually employed to test large structures such as offshore platforms. Figure 3 shows the basic experimental setup that was arranged in order to perform the step-relaxation test. The prototype was mounted on the steel base and this assemblage was fixed on the B&K 4801 vibration exciter table. During the entire test the exciter was maintained off, serving only as a fixed reference for the test item. The excitation mechanism consisted of a small piece of thin piano wire cord that was attached to the lumped mass at on end and to a fixed B&K 8001 impedance head ($340\,\mathrm{pC/N}$) at the opposite end. Once the static displacement was applied and the cord was cut, the built in force transducer on the impedance head registered the suddenly released force applied to the system. The beam's acceleration signals were captured by a B&K 4374 miniature accelerometer ($1.06\,\mathrm{pC/g}$) mounted at the lumped mass center of gravity. This sensor weighs approximately $0.64\,\mathrm{g}$, around $1\,\%$ of the lumped-mass m_o. Finally, the data acquisition system consists of two B&K 2626 charge amplifiers, one for the force signal and another one for the acceleration signal and the Agilent E1432 16 channels VXI data acquisition system with the MTS I-DEAS 10 software. A frequency range up to $200\,\mathrm{Hz}$ was covered during the tests, a total of 2048 data points was employed per interval, thus giving a $\triangle t = 0.005\,\mathrm{s}$ and $\triangle f = 0.097\,\mathrm{Hz}$ for the time interval between samples and frequency resolution, respectively.

Special attention must be paid to the signal processing of the force signal since the step function can not be Fourier transformed without significantly leakage. In order to reduce this source of error to a minimum, a simple procedure was employed in which both the input force and acceleration signals were AC coupled so that the DC offset in the measurement load is converted into an exponential impulse McConnell [8]. Another possibility would be by differentiating the analog time domain signals what would require special charge amplifiers which were not available at the time the tests were conducted. Figure 4 depicts the original measured input force and output acceleration time histories as well as the corresponding frequency spectra for both signals from the step-relaxation test. The time history for the input force essentially shows an impulse type of behavior what was expected since the signal was AC coupled. The output acceleration signal exhibits an exponential decay and does not decay out completely in the sixteen seconds time window and this can introduce leakage in the corresponding frequency domain signal. The bottom parts of fig. 4 shows the corresponding force and acceleration frequency spectra. The force frequency spectra shows a significant decay in the 0-200 Hz frequency range and this indicates potential problems with the excitation signal, that ideally should present a constant magnitude in the frequency domain for all frequencies. The experiment was repeated several times by changing the static load applied to the system as well as the length of the string connecting the beam to the impedance head. The results were similar to the ones showed here.

Another important point to mention is the fact that due to its mechanical nature, the step-relaxation allows a single time domain signal,and thus no averaging is possible. Therefore, it is expected that the measured input and output signals present some noise, despite the unit value for the coherence function! In order to reduce possible leakage problems specially due to the slow decaying of the acceleration signal, the classical solution proposed by McConnell [7] was employed, where transient and exponential window functions were applied to input and output signals, respectively. Figure 5 show the filtered time domain input and output signals as well as the corresponding frequency spectra.

Once the leakage error was reduced to a minimum through the windowing process the modified input and output signals were used to get the system's accelerance FRF. In this case the H1 was used since the input signal showed better values for

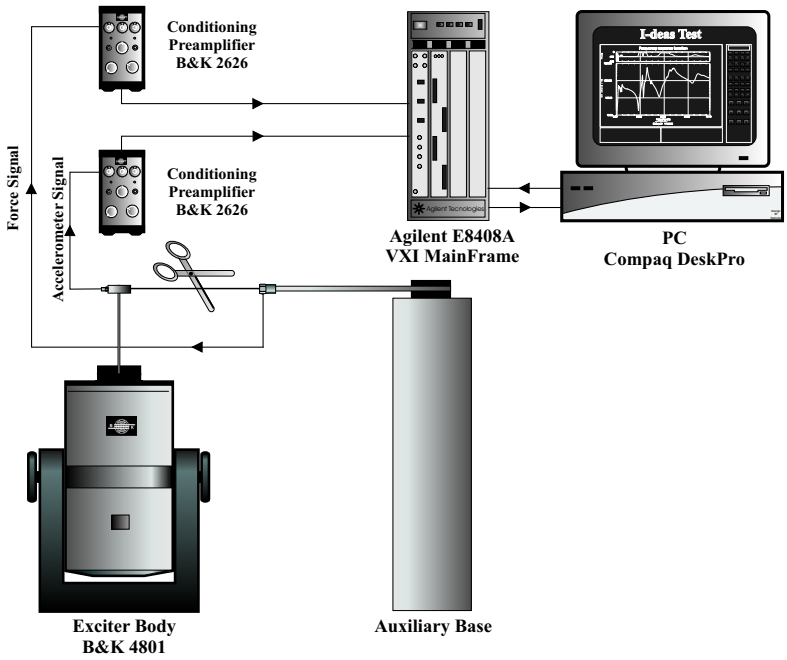

Figure 3 - The experimental layout employed to obtain the experimental classical response model for the transversal motion.

the signal to noise ratio as compared with the acceleration signal. From the calculated FRF, the MTS I-Deas 10 program was used to extract the following modal parameter: (i)damped natural frequency $\omega_d = 18.01\,\mathrm{Hz}$; (ii) measured damping factor $\zeta_m = 0.17\,\%$. The measured damping factor ζ_m represent the effect of the damping ratio ζ and the window damping ratio ζ_w [7], subtracting the effect of the exponential window used, result in $\zeta = 0.1272\,\%$.

Finally, the identified modal parameters are used to regenerate the accelerance FRF and the results are compared with the measured FRF as well as with theoretical FRFs calculated from the analytical model of the test structure. The results obtained are depicted on fig. 6. The comparison shown in fig. 6 also exhibits predicted FRFs for two different values for the lumped-mass m_o. The first value used comes from the lumped-mass plus the clamp bolts giving an equivalent mass of $63.6\,\mathrm{g}$. The second value used $m_o = 118\,\mathrm{g}$ comes from the best value of the lumped-mass in order to match with the experimental result, which can be claimed that for this value the theoretical and experimental curves matched very closely in the entire frequency range. On the other hand, the same behavior does not occur for the case where $m_o = 63.4\,\mathrm{g}$, even though this result also presents good agreement with the measured results.

The preceding sections of this article attempted to describe in details a process that has been around for several decades and that culminated with the response model of the test structure in terms of a single FRF. In a more extensive approach, a set of FRFs would be determined and the results would be given in terms of an FRF matrix for the structure. Also, the extracted FRF contains a single resonant frequency since the covered frequency range was limited to the 0-200 Hz range. Again, a more extensive analysis of the test structure would require that a wider range of frequencies be covered thus introducing extra degrees of freedom to the model.

Next, it will be presented an analysis with a different viewpoint aiming to demonstrate that depending on how the test structure is loaded in its dynamic environment the physical phenomenon shown might change significantly and the classical modal analysis principles do not apply anymore.

4 SECOND LEVEL OF ANALYSIS: FINITE AMPLITUDE OF VIBRATION

In the present section, the structure under investigation will be modelled in a similar manner as it was done before. First, a spatial model for the transversal motion will be derived and, later an approximated response model will de derived. Second, the prototype will be investigated from the experimental standpoint and the theoretical and experimental results will be

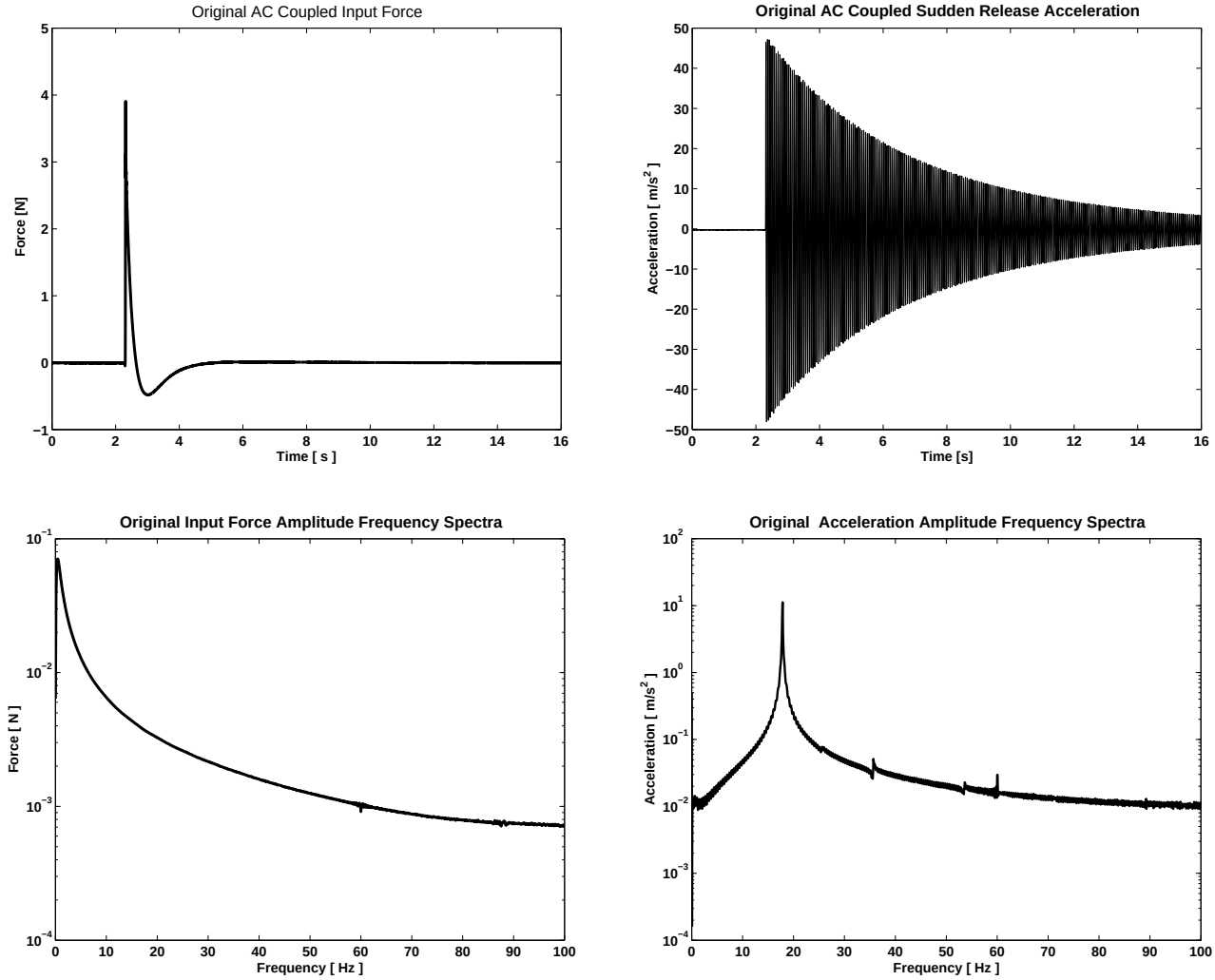

Figure 4 - Experimental measurements of the original signals of input force and output acceleration followed by their amplitude frequency spectra.

compared. However, in the present case the analysis will be carried out by assuming that the prototype can develop a finite amplitude of vibration [14]. In addition, instead of applying an excitation in the same direction as the of the resulting transverse motion, it will be applied a base excitation, which in turn is orthogonal to the transverse direction of motion. Figure 7 shows the physical model of the system for finite amplitudes

Based on fig.7, the transversal planar motion may be described by using the generalized coordinates $q_1(t) = u_o(t)$ and $q_2(t) = w_o(t)$, which describe the lateral displacement of the lumped mass and the axial contraction displacement of the lumped mass center, respectively. Let $u(z,t)$ denote the displacement as a function of z and the time t of the beam elastic axis, $W(t)$ the input displacement at the base, O' the center of the curvature ρ, ds, dz and $d\theta$ are, a infinitesimal distance on the beam, in the z direction and a infinitesimal angle, respectively.

4.1 Transversal Parametric Spatial Model of the Structure

When the prototype is subjected to the conditions stead above, a more realistic condition of finite amplitudes is considered where the total kinetic energy of the system is given as

$$T = \frac{1}{2} m_o (\dot{u_o}^2 + [\dot{w_o} - \dot{W}]^2) \tag{13}$$

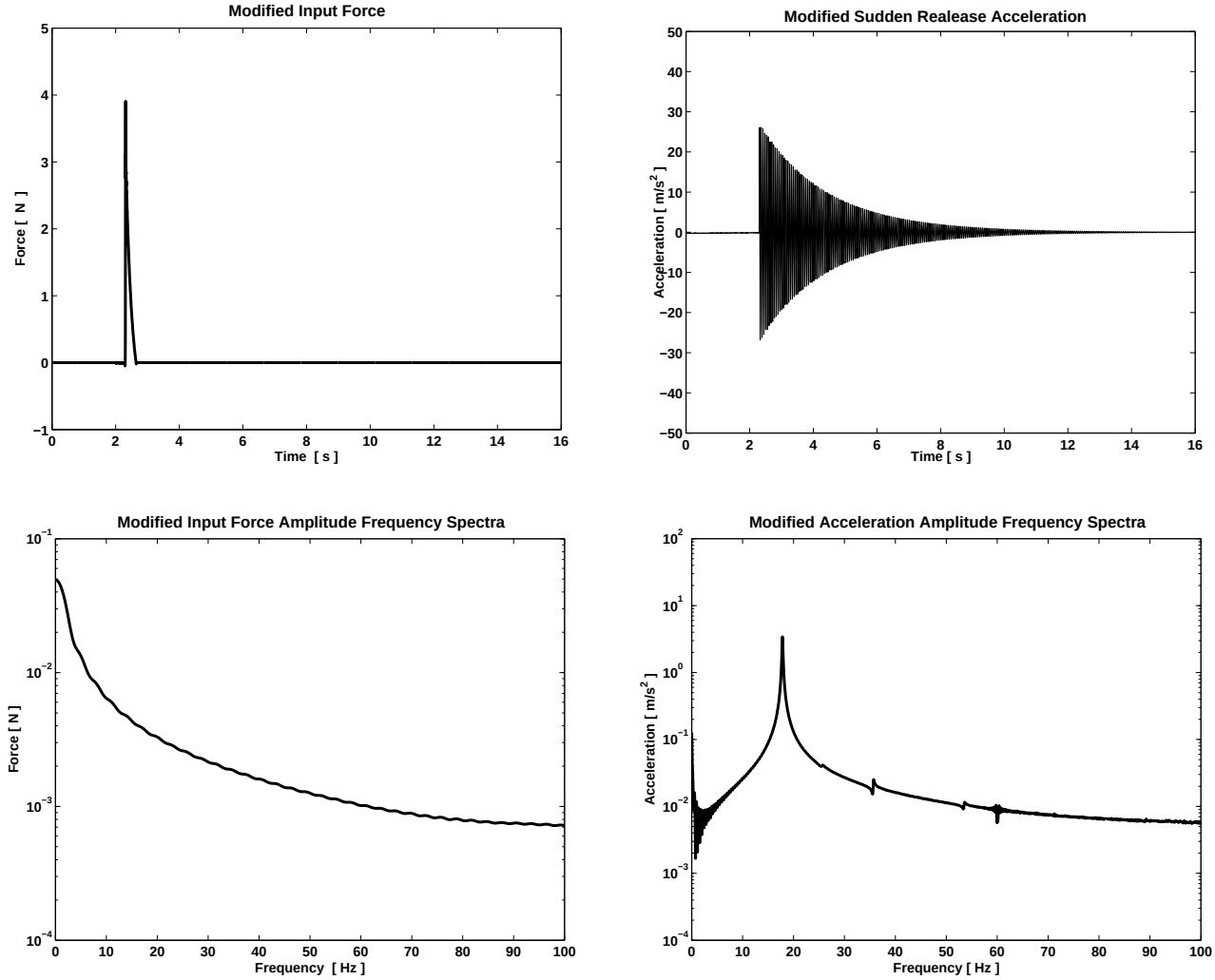

Figure 5 - Modified input force and output acceleration followed by their amplitude frequency spectra.

in which it can be noticed that there is no kinetic energy contribution due to rotary inertia of the lumped-mass. Also it can be noticed that there is a kinetic energy contribution due to the axial contraction w_o, since the trajectory of the lumped-mass is a semi-circle.

Before introducing the expression for the strain energy of the system under finite amplitude vibrations, it convenient to briefly discuss some aspects of the kinematics of the problem. The strain energy equation employed in the previous section, eq.2 has been obtained under some simplifying assumptions, and, all of them can be applied also in the case of finite amplitude except for the assumption for small curvature κ of the beam.

From fig.7 it can be obtained the geometric relationship between ρ,ds and $d\theta$ as $ds = \rho d\theta$, and by definition [5] the curvature $\kappa = 1/\rho$ or $\kappa = d\theta/ds$. If the curvature is sufficiently small so that $dz \approx ds$, then the eq.2 can be used, otherwise this equation is no longer applicable to the present case. Although, Anderson et al. [1] showed that the curvature of a cantilever beam plays a important role on its nonlinear dynamic response, it will be considered here that the strain energy can be described by eq.2 or as a function of the lateral displacement of the lumped-mass center $u_o(t)$ by

$$U = \frac{1}{2} EI_y \left[\int_0^L \left(f^{"} \right)^2 dz \right] u_o^2 - m_o g w_o \tag{14}$$

which also shows the contribution of the gravitational potential energy.

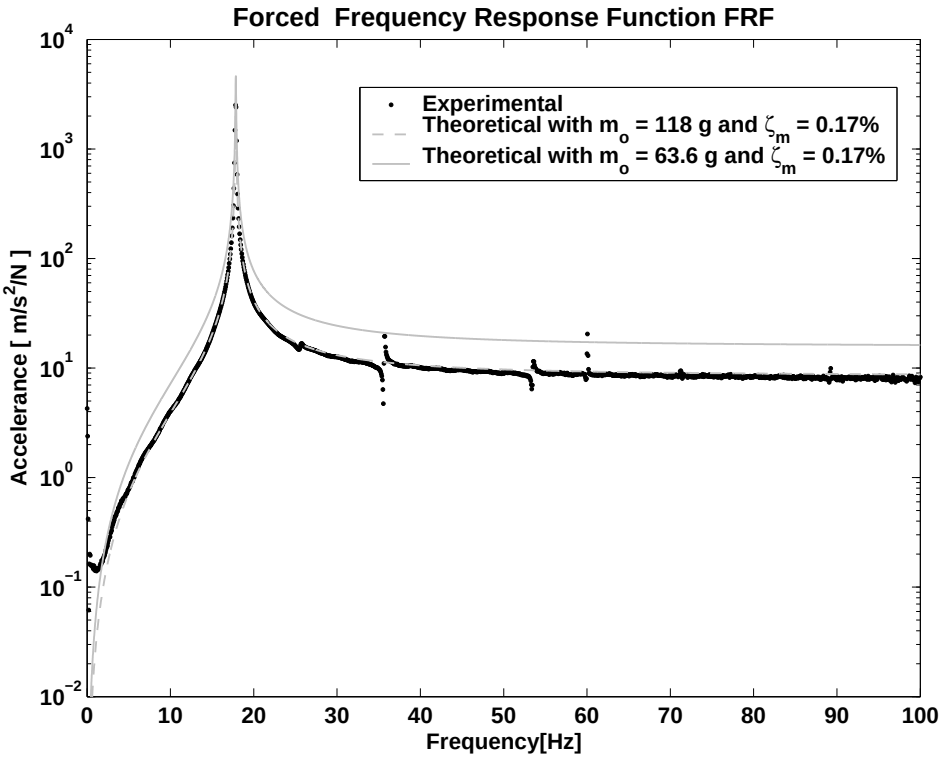

Figure 6 - Comparative results for the accelerance FRF for the test structure.

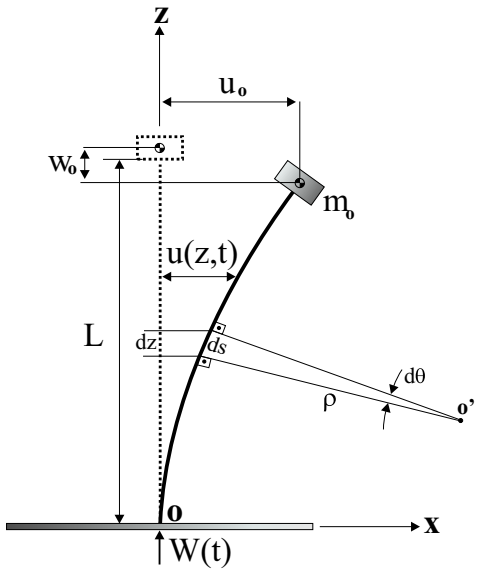

Figure 7 - Physical model of the structure under investigation, base excited and under the hypothesis of finite amplitude.

When the structure under investigation is under finite amplitude vibrations, it will be considered the action of two nonconservative forces. The first one, represent the structural damping and is modelled in terms of the generalized coordinates as $c_1 \dot{u}_o$, and the second one represents the drag damping acting on the system (when in motion) and is modelled in terms of generalized coordinates as proportional to the square of the velocity, or as $c_2 \dot{u}_0 \left|\dot{u}_0\right|$. Both forces act in the negative

direction of the virtual transversal displacement δu_o.

Therefore, the nonconservative virtual work δW_{nc} which is done on the system is given by $\delta W_{nc} = [-c_1\dot{u}_o - c_2\dot{u}_0\,|\dot{u}_0|]\,\delta u_o$. Since the nonconservative virtual work is defined as function of the nonconservative generalized force Q_{nc} as $\delta W_{nc} = Q_{nc}\delta u_o$, the nonconservative generalized force Q_{nc} is obtained as

$$Q_{nc} = \frac{\delta W_{nc}}{\delta u_o} = -c_1\dot{u}_o - c_2\dot{u}_0\,|\dot{u}_0| \tag{15}$$

Before applying the Lagrange's formulation to get the system's equation of motion, it is interesting to describe the total kinetic energy (eq.13) only in terms of the lateral velocity of the lumped-mass center $\dot{u_o}$ and the velocity of the base excitation $\dot{W}$. When the curvature is sufficiently small, the contraction displacement w is directly related to lateral displacement u by the eq.16 in which the primes denotes the partial derivation with respect to s

$$w = \frac{1}{2}\left[\int_0^L \left(u^{'}\right)^2 dz\right] \tag{16}$$

Substitution of eq.3 into eq.16 leads to describing the the contraction displacement w in terms of the contraction displacement w_o and the lateral displacement u_o, both of them related to the center of the lumped-mass m_o defined as

$$w_o = \frac{1}{2}\left[\int_0^L \left(f^{'}\right)^2 dz\right] u_o^2 \tag{17}$$

Differentiation of the eq.17 with respect to time finally leads to the eq.18.

$$\dot{w_o} = \left[\int_0^L \left(f^{'}\right)^2 dz\right] (u_o\dot{u_o}) \tag{18}$$

Equation 18 can be substituted into the eq.13 to yield

$$T = \frac{1}{2}m_o\dot{u}_o^2 + \frac{1}{2}m_o\left\{\left[\int_0^L (f')^2\,dz\right]^2 u_o^2\dot{u}_o^2 + \dot{W}^2 - 2\left[\int_0^L (f')^2\,dz\right] u_o\dot{u}_0\dot{W}\right\} \tag{19}$$

At this point the equation of the kinetic energy, potential energy and the work of the non-conservative forces can be used in the Lagrange's equation to get

$$\frac{d}{dt}\left(\frac{\partial T}{\partial \dot{u}_o}\right) - \frac{\partial T}{\partial u_o} + \frac{\partial V}{\partial u_o} = Q_{nc} \tag{20}$$

By performing each term of the Lagrange's equation and substituting the results in eq.20 the nonlinear spatial model of the system proposed under finite amplitude is derived, such final result is

$$\begin{aligned}&\left\{1 + \left[\int_0^L (f')^2\,dz\right]^2 u_o^2\right\} m_o\ddot{u}_0 + m_o\left[\int_0^L (f')^2\,dz\right]^2 u_o\dot{u}_o^2 + c\dot{u}_o + c_2\dot{u}_0\,|\dot{u}_0| + \\ &\quad + \left\{\tfrac{EI_y}{m_o}\left[\int_0^L (f'')^2\,dz\right] - \left[\int_0^L (f')^2\,dz\right]\ddot{W} - \left[\int_0^L (f')^2\,dz\right] g\right\} m_o u_o = 0\end{aligned} \tag{21}$$

It can be claimed in eq.21 that the gravitational term affects the undamped natural frequency of the system. However this influence is very small and it does not will be considered further herein. In addition, this nonlinear spatial model is yet an integro-differential equation and requires some manipulation before determination of the parametric response model of the test structure. As a first step in this direction the linear mode shape function $f(z)$ must be considered

$$f(z) = 1 - \cos\left[(2n-1)\,\frac{\pi z}{2L}\right] \tag{22}$$

where n is the number of the normal mode of the beam, that in the present case reduces to $n = 1$ [10]. Since the linear mode shape function $f(z)$ is known, the integrals in the nonlinear equation can be performed as shown the equations below, in which A and B are geometrical constants.

$$A = \int_0^L \left(f''\right)^2 dz = \left[\frac{\pi}{2L}\right]^4 \frac{L}{2} \tag{23}$$

$$B = \int_0^L \left(f'\right)^2 dz = \left[\frac{\pi}{2L}\right]^2 \frac{L}{2} \tag{24}$$

The displacement and acceleration of the base excitation are admitted as mono-component periodic functions with amplitude of the displacement Q and frequency Ω, mathematically expressed by

$$W(t) = Q\cos(\Omega t) \tag{25}$$

$$\ddot{W}(t) = -Q\Omega^2\cos(\Omega t) \tag{26}$$

Substitution of the geometrical constants A,B and the base acceleration $\ddot{W}$, dividing both sides by m_o, the nonlinear spatial model (21) can be rewriting as

$$\ddot{u}_0 + B^2\ddot{u}_0 u_o^2 + B^2 u_o \dot{u}_o^2 + \frac{c_1}{m_o}\dot{u}_0 + \frac{c_2}{m_o}\dot{u}_0\left|\dot{u}_0\right| + \frac{EI_y A}{m_o}u_o + \underbrace{\left[BQ\Omega^2\cos(\Omega t)\right]}_{Parametric\ Excitation}\ u_o = 0 \tag{27}$$

At this point, could be interesting bring back the spatial model for the transverse direction that has been obtained in the first level of analysis (item 3.1). This elementary spatial model is given originally by eq.7 and shown again below in an appropriated form

$$\ddot{u}_o + \frac{c_1}{m_o}\dot{u}_o + \frac{EI_y A}{m_o}u_o = \underbrace{\frac{F_o}{m_o}e^{i\Omega_e t}}_{External\ Excitation}$$

Comparison of these two spatial models reveals significant differences between them. First, the number of terms in the parametric spatial model is larger than in the forced spatial model, since there are seven terms in the nonlinear against four in the linear. In addition, the parametric spatial model has three nonlinear terms, namely two cross nonlinear terms, one involving the square of the displacement and the acceleration $B^2\ddot{u}_0 u_o^2$ and other involving the displacement and the square of the velocity $B^2 u_o \dot{u}_o^2$, and one purely nonlinear involving the square of the velocity $\frac{c_2}{m_o}\dot{u}_0\left|\dot{u}_0\right|$. Furthermore, it can be seen the forced spatial model is a linear-time-invariant (LTI) model, and represented by a second order linear non-homogeneous differential equation. On the other hand, the parametric spatial model is a nonlinear-time-variant (NLTV) model, and represented by a nonlinear time variant differential equation.

Even though they are so different in nature, there are some common terms between them. Both of them present: (i) a linear term representing the purely inertial force $\ddot{u}_0$; (ii) a linear term representing the structural damping $\frac{c_1}{m_o}\dot{u}_o$; (iii) a linear term representing the linear elastic force $\frac{EI_y A}{m_o}u_o$. Since that the parametric spatial model has been obtained, it will be possible to obtain its the parametric response model. This development is shown in the next section.

4.2 Transversal Parametric Response Model of the Structure

The first level of analysis presented on this article has employed the classical modal analysis approach in order to obtain the system's response model based on the spatial characteristics of the test structure and an appropriate input. However, in present level of analysis the spatial model is much more complex and characterized by a nonlinear time-variant mathematical

model as given by eq. 27. Hence, the standard method no longer can be applied and a more dedicated mathematical tool must be employed to obtain the parametric response of the nonlinear system. The classical theory of nonlinear vibration usually classifies the solution methods in three main group: exact methods, approximated analytical techniques, and numerical methods. In the present study it will be employed an approximated analytical technique, known as method of multiple scales ([12]).

In order to adequately perform the analysis using the method of multiple scales, first it is necessary to transform the parametric spatial model given by eq.27 into a dimensionless form followed by ordering the terms in this dimensionless equation according to the importance of each one on the global dynamic behavior of the system. Proceeding in this form, the ordered dimensionless parametric spatial model can be written as

$$\epsilon^0 \ddot{u}_0^* + \epsilon^2 \ddot{u}_0^* u_o^{*2} + \epsilon^2 u_o^* \dot{u}_o^{*2} + \epsilon^1 C_1 \dot{u}_o^* + \epsilon^1 C_2 \dot{u}_o^* \left|\dot{u}_o^*\right| + \epsilon^0 u_o^* + \epsilon^1 D \cos\left(\phi t^*\right) u_o^* = 0 \tag{28}$$

whereby ϵ is a small parameter ($\epsilon \ll 0$), u_o^* to be the new dimensionless lateral displacement and t^* the dimensionless time (independent variable, not explicitly). From the dimensionless process, $u_o^* = B u_o$ and $t^* = \frac{t}{T_n}$, whereby B it is a constant of geometric nature and T_n is the linear undamped natural period. Furthermore, the ordered dimensionless coefficients $\epsilon^1 C_1$, $\epsilon^1 C_2$ and $\epsilon^1 D$ as well as the frequency ratio between the parametric frequency Ω and the undamped natural frequency ω_n, represented by ϕ, are given as

$$\epsilon^1 C_1 = \frac{c_1 T_n}{m_o} \qquad \epsilon^1 C_2 = \frac{c_2}{m_o B} \qquad \phi = \frac{\Omega}{\omega_n} \qquad \epsilon^1 D = Q B \phi^2 \tag{29}$$

By examining eq.28, it can be noticed that the first term $\ddot{u}_0^*$ represents the inertia term, which is fundamental in the dynamic behavior of the system and it is then considered to be "strong". This is similarly true for the sixth term u_o^* that represents the stiffness term. Both, the inertia and the stiffness terms could be regarded as being of zero order (unaltered) and could be rewritten for the sake of mathematical completeness as $\epsilon^0 \ddot{u}_0^*$ and $\epsilon^0 u_o^*$. On the next level are consider those terms that dictate the flow of the excitation energy through the system: (i) the parametric excitation; (ii) the damping terms. Both of them could be regarded as being of first order and rewritten as $\epsilon^1 C_1 \dot{u}_o^*$, $\epsilon^1 C_2 \dot{u}_o^* \left|\dot{u}_o^*\right|$ and $\epsilon^1 D \cos\left(\phi t^*\right) u_o^*$. The remaining terms $\ddot{u}_0^* u_o^{*2}$ and $u_o^* \dot{u}_o^{*2}$ are nonlinear and their contribution to the principal parametric resonance condition is likely to be negligible, although a sensitive high-order analysis could reveal some small contribution arising from these terms. As a result, these terms are neglected in a relative sense, as being small terms. Furthermore this "small" is accentuated by the presence of derivatives and for these reasons these terms could be made as second-order terms ϵ and rewritten as $\epsilon^2 \ddot{u}_0^* u_o^{*2}$ and $\epsilon^2 u_o^* \dot{u}_o^{*2}$.

The mathematical development using the method of multiple scales in order to find a approximated solution of the eq.28 is very extensive and relatively complex to be entirely described in the present article, therefore this procedure will not be shown in greater details. However it will be provided the minimum description of the method so that the the major steps of this procedure can be followed. First, attention is focused on the characteristics of the prototype at the principal parametric resonance. As it is known ([14],[11]) this phenomenon occurs when the parametric excitation Ω assumes a value equal to the double of the undamped natural frequency ω_n. The ratio between Ω and ω_n has already been defined as $\phi = \Omega/\omega_n$, therefore at the principal parametric resonance ϕ can be written as $\phi = 2 + \varepsilon\sigma$, in which $\varepsilon\sigma$ is a detuning parameter that express the proximity of the principal parametric resonance. Second, the method of multiple scales has been employed to find the first approximation of the solution of eq.28. The final result obtained, considering a first order approximation in the neighborhood of the principal parametric resonance is given by

$$u_o^*\left(\epsilon, t^*\right) = a(T_1) cos(T_0 + \beta(T_1)) + \ldots \tag{30}$$

where $T_0 = t^*$ is a fast scale associated with changes at the frequency ϕ, and $T_1 = \epsilon t^*$ is a slow scale associated with modulations in the amplitude and phase caused by the damping, resonance and nonlinear characteristics. In addition, the amplitude $a(T_1)$ and the phase $\beta(T_1)$ are given by

$$\frac{da}{dT_1} = -\frac{1}{2} a C_1 - \frac{1}{4} D a \sin\left(\sigma\, T_1 - 2\,\beta\right) - \frac{4 a^2 C_2}{3\pi} \tag{31}$$

$$a \frac{d\beta}{dT_1} = \frac{1}{4} D a \cos\left(\sigma\, T_1 - 2\,\beta\right) \tag{32}$$

Since an approximated response is known, the parametric response model can be finally derived, initially by transforming the equations (31) and (32) into an autonomous system (i.e., one in which T_1 does not appear explicitly) by letting $\Gamma = \sigma T_1 - 2\beta$ and the result is

$$\frac{da}{dT_1} = -\frac{1}{2}aC_1 - \frac{4a^2C_2}{3\pi} - \frac{1}{4}Da\sin(\Gamma) \tag{33}$$

$$a\frac{d\Gamma}{dT_1} = a\sigma - \frac{1}{2}Da\cos(\Gamma) \tag{34}$$

The steady-state motions of the eq.28 correspond to the fixed points (i.e. constant solutions) of the equations (33) and (34), which in turn correspond to $\frac{da}{dT_1} = \frac{d\Gamma}{dT_1} = 0$. Multiplying by ϵ^1, then squaring and at the end adding the equations (33) and (34), the following result is obtained

$$\tilde{a}^2\left[\left(\epsilon^1 C_1 + \frac{8\tilde{a}\epsilon^1 C_2}{3\pi}\right)^2 + (\epsilon^1\sigma)^2\right] = \frac{1}{4}(\epsilon^1 D)^2\tilde{a}^2\left[\sin^2(\Gamma) + \cos^2(\Gamma)\right] \tag{35}$$

where $\tilde{a}$ means steady-state amplitude. It follows that the solution for the steady state dimensionless amplitude of of the transverse motion $\tilde{a}$ due the parametric excitation in the longitudinal direction is given by both $\tilde{a}^2 = 0$ and

$$\tilde{a} = -\frac{3\pi\epsilon^1 C_1}{8\epsilon^1 C_2} \pm \frac{3\pi}{16\epsilon^1 C_2}\left\{-4(\epsilon^1\sigma)^2 + \left[\epsilon^1 QB\left(2+\epsilon\sigma\right)^2\right]^2\right\}^{1/2} \tag{36}$$

where D has been replaced by $QB\phi^2$ and after ϕ^2 with $(2+\epsilon\sigma)^2$. Dividing both sides of eq.36 by the dimensionless variable $\epsilon^1 QB$, which in turn represents de base's displacement gives

$$OTR(\epsilon^1 QB, \phi) = \frac{\tilde{a}}{\epsilon^1 QB} = -\frac{3\pi\epsilon^1 C_1}{8\epsilon^1 QB\epsilon^1 C_2} \pm \frac{3\pi}{16\epsilon^1 QB\epsilon^1 C_2}\left\{-4(\epsilon^1\sigma)^2 + \left[\epsilon^1 QB\left(2+\epsilon\sigma\right)^2\right]^2\right\}^{1/2} \tag{37}$$

Physically eq.37 describes how the transverse motion is affected by the longitudinal base's motion when the prototype is subjected to the principal parametric resonance. Thus, this parametric response model will be further called by Orthogonal Transmissibility Ratio (OTR). In addition while the classical forced response model is completely independent of the amplitude's force, this is no longer valid for the parametric response model. Equation37 shows that the OTR is a function of both, the frequency of the parametric excitation in the neighbor of the principal parametric resonance (represented by the dimensionless variable ϕ), and the amplitude of the parametric excitation (represented by the dimensionless variable $\epsilon^1 QB$). Furthermore, this equation still shows that the transverse vibration occur due to longitudinal excitation at a frequency that is double of the transverse natural frequency !. All these theoretical aspects will be confirmed in the experimental tests on the prototype, in which will be shown in the next section

4.3 Experimental Parametric Response Model of the Structure

In order to experimentally obtain the Orthogonal Transmissibility Ratio (OTR) for the prototype tested, the test setup shown in fig.8 was used. In this test, the beam-lumped mass system and its mounting base are attached to the table of the B&K 4810 vibration exciter that will provide the base driven excitation signal to the test structure. The base driven test was chosen here for two main reasons: (i) to illustrate an experimental situation where the principal parametric resonance occurs and (ii) to simulate a field dynamic environment where the test structure not necessarily is excited according to the main direction of vibration. The Agilent E1432A DSP board mounted on the Agilent E8408A mainframe is used to perform three major tasks during the test: (i) generation of the signal that will be sent to the exciter through the B&K 2707 power amplifier; (ii) control of this excitation signal so that no significant variation of the exciter's table motion occurs during the test and; (iii) acquisition of all measured signals. The MTS I-Deas 10 software is used as the interface measurement program to perform all these tasks.

Two linear single axis accelerometers are used in the test, one of them, the B&K 4374 ($1.06\,\mathrm{pC/g}$) and mass of $0.64\,\mathrm{g}$ is attached to the beam's lumped mass and will measure the transverse motion due to the base driven acceleration signal.

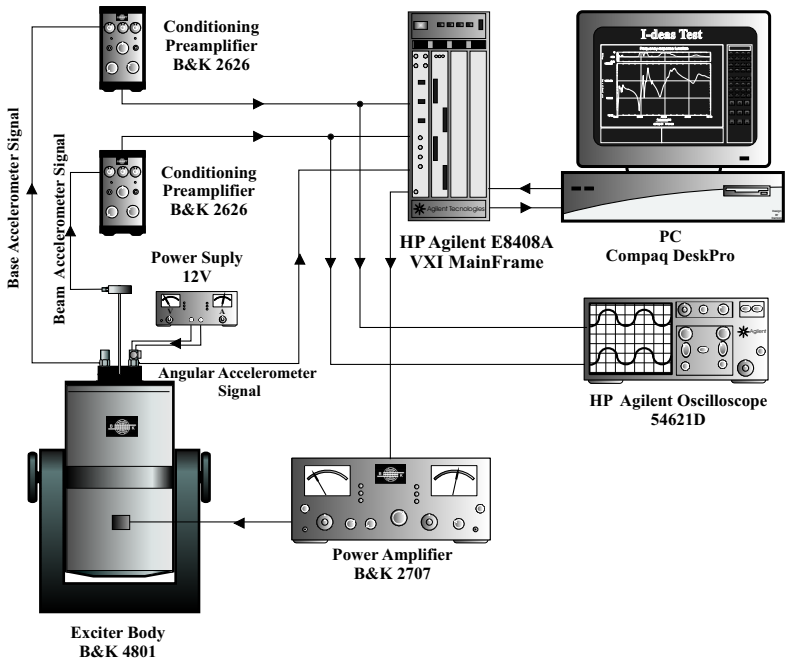

Figure 8 - The experimental layout employed to obtain the experimental parametric response model (OTR).

The second linear single axis accelerometer, a B&K 4371($9.84\,\mathrm{pC/g}$) is attached to the mounting base and is used to monitor the input base signal and is also the signal used as feed back to the data acquisition signal in order to perform the closed loop control to mantain the input base acceleration signal constant during the test. A third accelerometer, the angular Kistler 8836M01 ($34\,\mu\mathrm{V/rad/s^2}$) is also mounted on the base of the structure and is used to monitor possible rocking motions presented by the exciter's suspension system. Although the B&K 4810 exciter is very stable as far as armature's rocking motions are concerned, there is always the possibility of small geometric misalignments in base driven tests which can sometimes induce some rocking motions on the exciter's armature. The linear accelerometer signals are conditioned by B&K 2626 charge amplifiers prior to the data acquisition signals. The signals are also monitored by the HP 54621D digital oscilloscope.

Once all the instrumentation is properly set, the next step is to define a testing strategy, that begins by choosing a suitable excitation signal. Since the major goal is to predict nonlinear behavior of the test structure, two tests are planned using a sine dwell excitation signal to drive the test structure. The first test is performed by adjusting the excitation level such that a $39.24\,\mathrm{m/s^2}$ amplitude signal is obtained. Then frequency is varied upward and downward and the values of the resulting transverse acceleration at the beam's tip mass are recorded in both directions of the varying excitation frequency. The second test is identical to the first one, except that in this case, the amplitude of the base driven signal is changed to $29.43\,\mathrm{m/s^2}$. During all tests the base motion measured by the linear accelerometer is constantly monitored and fed into the data acquisition system as the reference signal to be controlled.

Figure9 shows the resulting transverse motion measured at the beam's tip mass for the case where the base amplitude motion is $39.24\,\mathrm{m/s^2}RMS$ and the excitation frequency is set at a value approximately double of the cantilever undamped natural frequency of the beam-lumped mass system. This is just the parametric resonance condition as observed in fig.9. In this signal it can be noticed that, for this condition, the steady-state condition is reached at approximated $10\,\mathrm{s}$, therefore a waiting time about three times this value was further used to guarantee that the transient vanishes completely and the system reaches the steady state condition every time the excitation signal is varied.

Figure10 shows the results of the base acceleration amplitude control obtained during the tests. As seen from this figure, excellent results were obtained in keeping the base at constant amplitude for both amplitudes tested. The relative mean error found to the base acceleration at $29.46\,\mathrm{m/s^2}RMS$ is only 0.92% in the upward sweep and 1.06% in the downward sweep. Also, a small relative error has been also found for acceleration of the base at $39.24\,\mathrm{m/s^2}RMS$, mean of 0.78% in the upward sweep and 0.73% in the downward sweep.

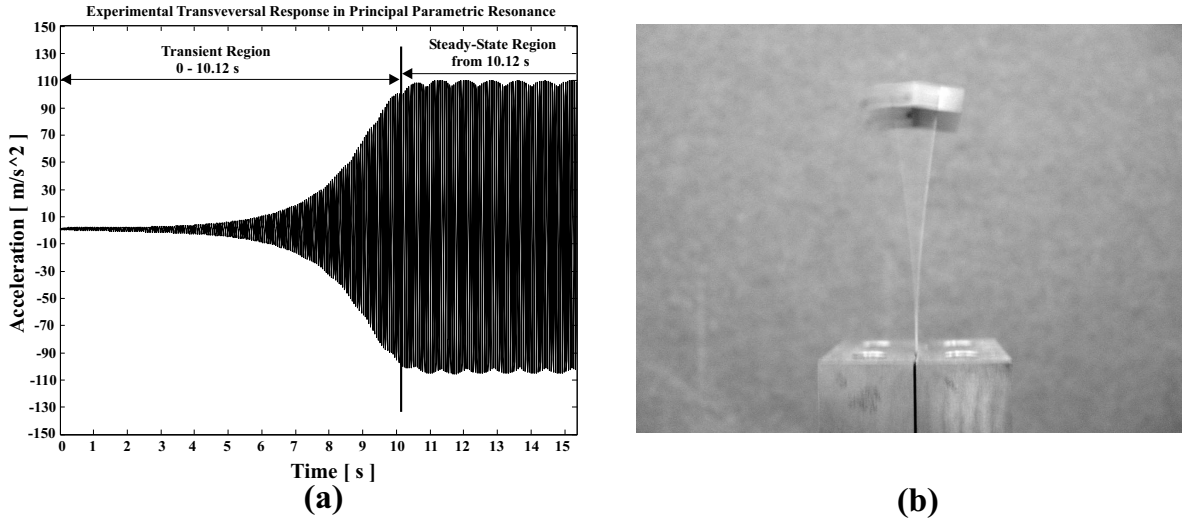

Figure 9 - The experimental transversal response of the prototype when in principal parametric resonance for magnitude of base acceleration of $39.24\,\mathrm{m/s^2}RMS$: (a) temporal signal; (b) prototype in the principal parametric resonance (steady-state).

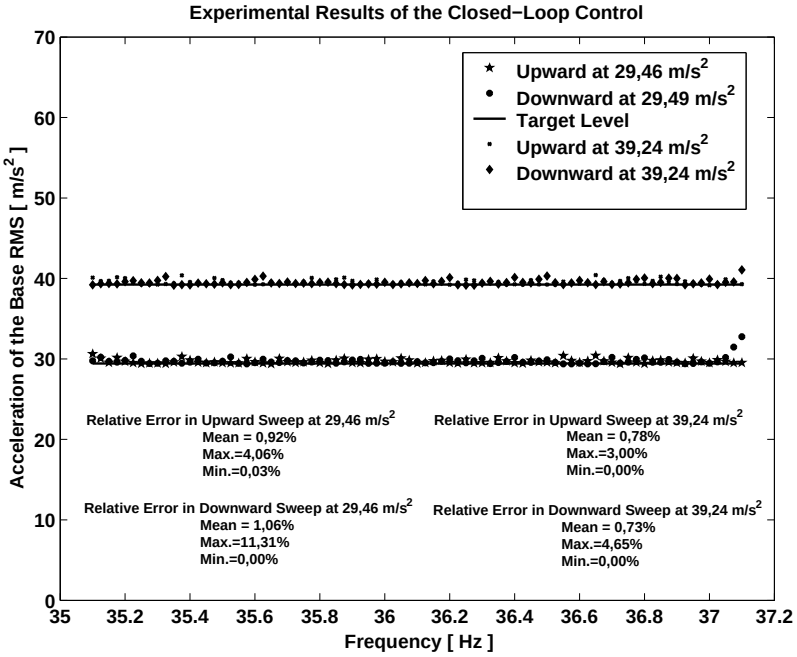

Figure 10 - Experimental amplitude control results for the base driven acceleration signal

Figure11 shows the results for the angular acceleration measurements obtained during the tests. As it can be seen from the results, some rotation of the base was observed and they are primarily due to small geometric misalignments with respect to the exciter's vertical axis and also possible unstable behavior of the exciter suspension system.

Since at the moment the tests were performed no procedure was available to quantify the influence of the base rocking motion on the transverse linear acceleration, a qualitative analysis was done by comparing the theoretical response obtained from the numerical solution of equations (equations 31 and 32) with the experimental response obtained from the test. Figure12 shows this comparison and a good agrement between exists between numerical and experimental results, even

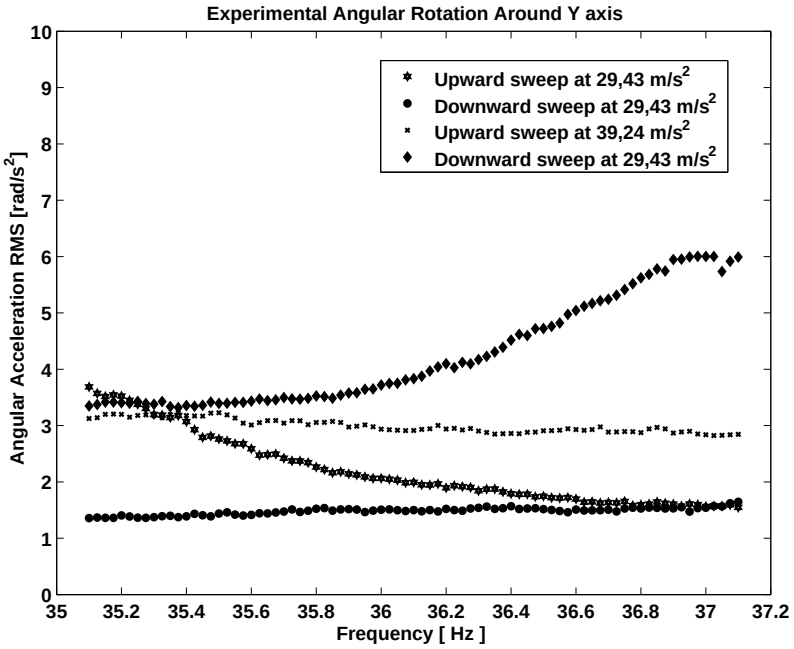

Figure 11 - The experimental angular acceleration around the Y axis, obtained during the tests.

though the experimental results exhibits an amplitude modulation in the the steady-state response, which could result from either the base's rotation or other nonlinearities not considered in the theoretical model.

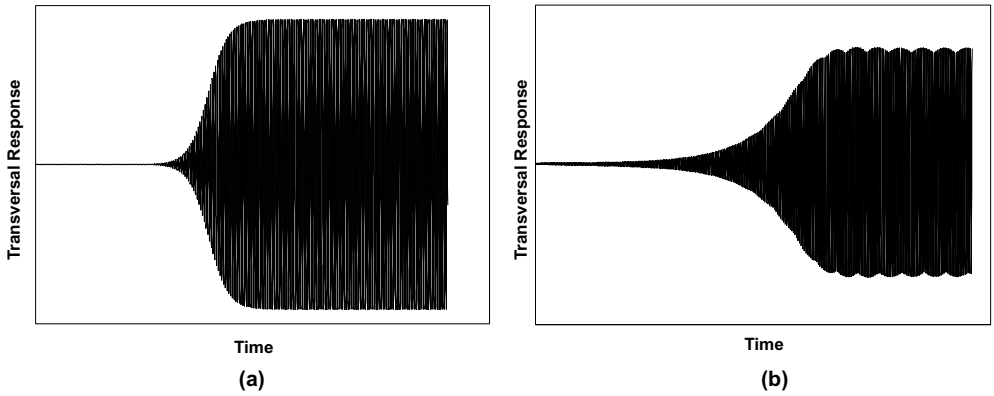

Figure 12 - Qualitative comparison between theoretical response (a) and experimental response (b) for the principal parametric resonance. Theoretical result obtained with $\epsilon^1 C_1 = 0.0025$; $\epsilon^1 C_2 = 0.0041$; $\epsilon^1 D = 0.0533$ and experimental result for base's amplitude at $39.24\,\mathrm{m/s^2} RMS$ and $36.07\,\mathrm{Hz}$.

The experimental parametric response model here represented by the OTRs are shown in figures 13 and 14. In addition, theoretical OTRs are also shown in each figure for comparison purposes. It can be concluded from this comparison that either the experiment needs further improvements and the theoretical model also needs to be updated before the experimental and theoretical results can match. Furthermore, it can be conclude, specially from fig.13 that the curvature of the beam indeed plays a important role in the response of the prototype as it is observed for example in the downward sweep. In addition, the influence of the amplitude of the parametric excitation in the OTR is experimentally proved. By comparing the figures 13 and 14 it can be seen that with the increase of the amplitude of the parametric excitation the shape of the OTR has changed considerably

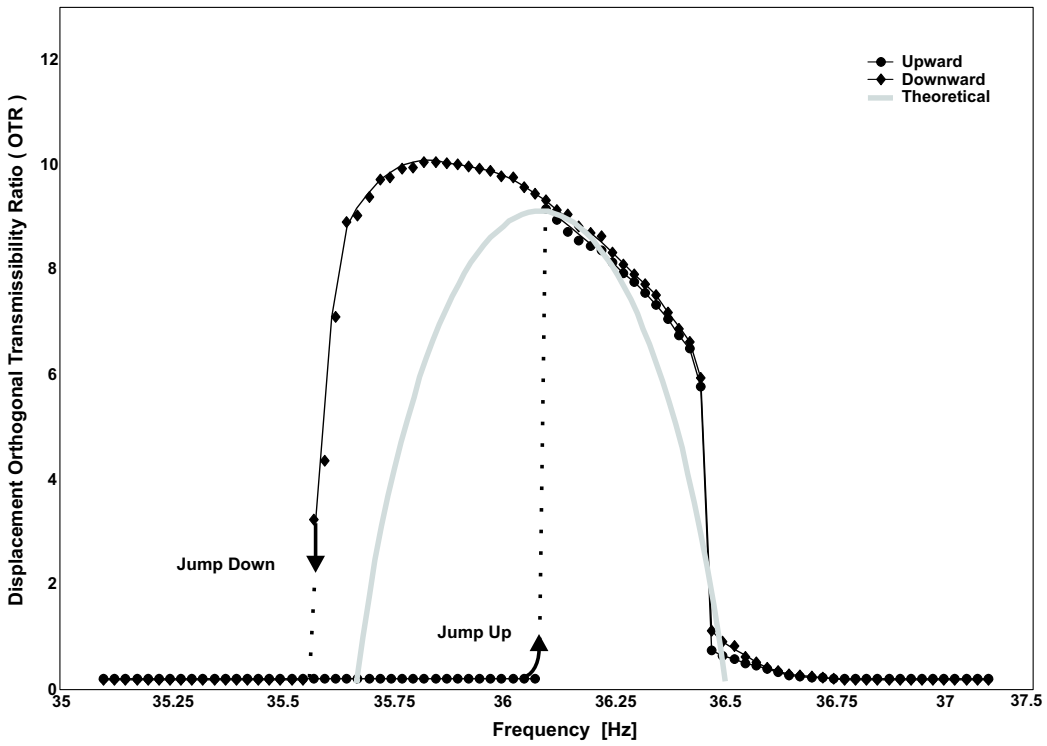

Figure 13 - Experimental and Theoretical Orthogonal Transmissibility Radio, in which represent the parametric response model. Experimental OTR obtained for base's amplitude at $1.1\,\mathrm{mm}[Peak]$ or $(39.24\,\mathrm{m/s^2}\,[RMS]{*}\sqrt{2}\,@\simeq 36\,\mathrm{Hz})$. Theoretical OTR obtained with $\epsilon^1 C_1 = 0.0160$; $\epsilon^1 C_2 = 0.1598$; $\epsilon^1 QB = 0.0134$ and $\epsilon^1 = 0.8$.

As mentioned in the nonlinear theory, indeed the direction of the sine-dwell really changed the OTR's shape for the testing structure, however it is important to point out that this feature might not be present in other structures. Particularly, the prototype tested here has two stable responses in the tested frequency range, what is a key factor in changing the shape of the OTR when the frequency is dwelled upward or downward

Finally, while classical transmissibility ratio for linear system models is independent of the physical quantities employed, namely acceleration, velocity or displacement, the same does not occur with the orthogonal transmissibility ratio (OTR). The OTR has the peculiar characteristic of showing different amplitudes depending on the physical quantities used.

5 CONCLUDING REMARKS

Every day, the industries around the world are looking for better and cheaper results. Since the modal testing procedures require sophisticated computer based instrumentation, a good number of well trained personnel, and also, depending on the complexity of the tested structure tends to be time consuming, it is a very expensive item in most industries budgets. Frequently, the modal analyst do not have enough time or more dedicated instrumentation and training to explore something that runs away from the trivial classical analysis. On the other hand, the increased requirements on the speed, power, long life, reliability and smaller weight impose higher vibration levels to the structure. Hence, there will be situations where nonlinear effects will become more and more important, drawing the attention of testing personnel. In this article, one of these nonlinear effects was subject of a detailed study from both the theoretical and experimental viewpoints. Classical modal analysis approaches were utilized to identify major and important characteristics of the test structure by assuming linearity as a valid framework. The system was successfully identified, proving that the classical theoretical and experimental modal analysis procedure plays a crucial role in understanding the structure dynamic behavior. However, it was also demonstrated that a simple change on the excitation direction and amplitude revealed very important dynamics, not observed in the previous analysis using the classical method. Hence, in a field application, depending on the excitation condition, the classical response model might reveal insufficient to fully describe the structure's dynamics.

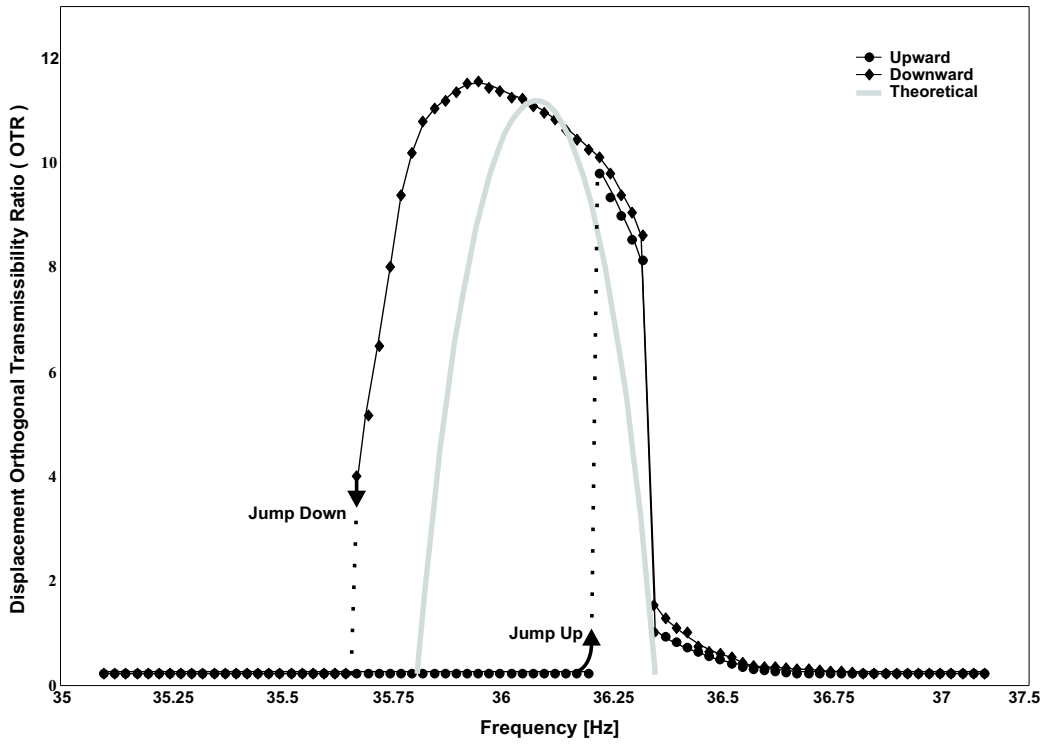

Figure 14 - Experimental and Theoretical Orthogonal Transmissibility Radio, in which represent the parametric response model. Experimental OTR obtained for base's amplitude at $0.81\,\mathrm{mm}[Peak]$ or $(29.3\,\mathrm{m/s^2}\,[RMS]*\sqrt{2}\,@\simeq 36\,\mathrm{Hz})$. Theoretical OTR obtained with $\epsilon^1 C_1 = 0.0160$; $\epsilon^1 C_2 = 0.0879$; $\epsilon^1 QB = 0.0100$ and $\epsilon^1 = 0.9$.

During the experimental work developed here, it could be observed the importance of the principal parametric resonance phenomenon, which in a given condition subjected the structure to a very high vibration level. In addition, the theoretical spatial and response models to describe this phenomenon are much more complex than the corresponding classical models, requiring more complex mathematical tools to describe it, and in practice only an approximate solution is found. Evidently all these complications are amplified when the structure under investigation is more complex, presenting many more degrees of freedom.

6 ACKNOWLEDGMENTS

The authors gratefully acknowledge the support given to the reported reseach by the Conselho Nacional de Desenvolvimento Científico e Tecnológico, CNPq, Brazil. The Laboratory support received from University of Sao Paulo is greatly appreciated. Most of data measurement and processing was possible due to the valuable support received from MTS Corporation through I-Deas Test software. Kistler is also kindly acknowledged for providing the angular piezoelectric accelerometer.

7 REFERENCES

[1] T J ANDERSON, A H NAYFEH, and B BALACHANDRAN. Experimental verification of the importance of the nonlinear curvature in the response of a cantilever beam. *Journal of Vibration and Acoustics*, 118:21–27, 1996.

[2] M CARTMELL. *Introduction to linear, parametric and nonlinear vibration*. Chapman and Hall, London, 1990.

[3] R M EVAN-IWANOWSKI. On the parametric response of structures. *Applied Mechanics Reviews*, 18(9):699–702, 1965.

[4] D J EWINS. *Modal testing: Theory and Pratice*. Research Studies Press LTD, London, 1986.

[5] J M GERE and S P TIMOSHENKO. *Mechanical of materials*. PWS, Boston, 4ed. edition, 1997.

[6] N M M MAIA and J M M SILVA. *Theoretical and Experimental Modal Analysis*. Wiley & Sons, New York, 1997.

[7] K G McCONNELL. *Vibration Testing: Theory and Pratice*. Wiley & Sons, New York, 1995.

[8] K G McCONNELL and P J SHERMAN. Frf estimation under non-zero initial conditions. In *Proceeding of the 11th International Modal Analysis Conference*, page 8, Kissimmee, 1993. USA, SEM.

[9] L MEIROVITCH. *Introduction to dynamics and control*. Wiley & Sons, New York, 1985.

[10] L MEIROVITCH. *Elements of vibration analysis*. McGraw-Hill, New York, 1986.

[11] N MINORSKI. *Nonlinear oscillations*. Van Nostrand Reinhold, Princeton, 1962.

[12] A H NAYFEH. *Pertubation Methods*. Wiley & Sons, New York, 1973.

[13] A H NAYFEH. *Nonlinear Interactions: Analytical, Computational, and Experimental Methods*. Wiley & Sons, New York, 2000.

[14] A H NAYFEH and D T MOOK. *Nonlinear oscillations*. Wiley & Sons, New York, 1979.

[15] J S RAO. *Advanced theory of vibration*. Wiley & Sons, New York, 1992.

[16] S S RAO. *Mechanical vibrations*. Addison-Wesley, New York, 1995.

[17] R M ROSENBERG. *Analytical dynamics of discrete systems*. Plenum-Press, New York, 1977.